New Journal of Physics
The open-access journal for physics

Radiation pressure acceleration of thin foils with circularly polarized laser pulses

A P L Robinson[1], M Zepf[2], S Kar[2], R G Evans[1,3] and C Bellei[3]

[1] Central Laser Facility, STFC Rutherford-Appleton Laboratory, Chilton, OX11 0QX, UK
[2] Department of Physics and Astronomy, Queen's University Belfast, BT7 1NN, UK
[3] Plasma Physics Group, Blackett Laboratory, Imperial College London, SW7 2BZ, UK
E-mail: m.zepf@qub.ac.uk

New Journal of Physics **10** (2008) 013021 (13pp)
Received 31 August 2007
Published 21 January 2008
Online at http://www.njp.org/
doi:10.1088/1367-2630/10/1/013021

Abstract. A new regime is described for radiation pressure acceleration of a thin foil by an intense laser beam of above 10^{20} W cm^{-2}. Highly monoenergetic proton beams extending to giga-electron-volt energies can be produced with very high efficiency using circularly polarized light. The proton beams have a very small divergence angle ($<4^{\circ}$). This new method allows the construction of ultra-compact proton and ion accelerators with ultra-short particle bursts.

Contents

1. Introduction

Since the pioneering work of Clark *et al* [1], Maksimchuk *et al* [2], and the studies done with the Nova PetaWatt laser [3, 4], there has been considerable interest in the generation of multi-mega-electron-volt proton beams from thin foil targets irradiated by ultraintense lasers [5]–[12]. This interest is driven by some outstanding qualities of these beams due to their very low emittance [10], short burst duration and the very large accelerating field ($>10^{12}\,\mathrm{V\,m^{-1}}$). The large accelerating field allows ions to be acclerated to mega-electron-volt type energies over micron length scales and hence, allows the construction of ultra compact accelerators. Potential applications that might benefit from an accelerator with such properties are fast ignition inerital confinement fusion (ICF) [13]–[15] and radiotherapy for the treatment of tumours and probing laser-plasma interactions [16]. Currently, the extremely low emittance is achieved by a combination of large divergence with a small source size and short burst duration with a 100% energy spread. Any novel scheme that can reduce the divergence and produce monoenergetic beams would therefore present a very substantial breakthrough. In experiments to date the acceleration normally attributed to target normal sheath acceleration (TNSA) [6], [17]–[20]. In TNSA, the acceleration of the initially cold ions is due to the strong fields set-up by a sheath of laser accelerated relativistic electrons at the rear of the foil. The ion energy is dominated by the temperature and density of the hot electron population and hence scales as $(I\lambda^2)^{1/2}$.

Another, in principle very efficient means of using lasers to accelerate foils to high velocities has been discussed in the literature for many years [21]—radiation pressure acceleration (RPA). Hereby, the momentum of the laser is imparted directly to the object to be accelerated. Simple analytic models based on momentum conservation indicate that the final energy should simply scale as $\propto (I\tau/\sigma)^{\alpha}$ (where I is the intensity, τ the pulse duration and σ is the areal mass of the foil). The exponent, α is equal to 2 for $v_{\mathrm{final}} \ll c$, and $\alpha \to 1/3$ in the ultrarelativistic limit. In terms of simple numbers, any laser capable of $>10^7\,\mathrm{J\,cm^{-2}}$ should therefore be able to accelerate sub-micron foils to a monoenergetic beam with energies in excess of 1 MeV and should provide a much more favourable intensity scaling than TNSA (which scales $\propto I^{1/2}$) in most cases. However, this has never been demonstrated for realistic parameters above the plasma formation threshold.

While high power lasers that can deliver $>10^7\,\mathrm{J\,cm^{-2}}$ in a variety of pulse durations and wavelengths have existed for decades, there is no experimental evidence of RPA actually being the dominant process anywhere in this wide parameter range. For example, for lasers with $>10^{15}\,\mathrm{W\,cm^{-2}}$ and 10 ns duration, foil acceleration is ablatively driven [22] and for CPA lasers with $>10^{19}\,\mathrm{W\,cm^{-2}}$ and <1 ps TNSA is the dominant particle acceleration mechanism [4]. The question is therefore, whether there is any scheme for realistic laser parameters in which RPA can be expected to dominate. Recently, this area has been invigorated by the numerical demonstration of RPA by Esirkepov *et al* [23] at $I > 10^{23}\,\mathrm{W\,cm^{-2}}$ using linear polarization. Unfortunately, this high intensity will preclude the possibility of testing this theory for a number of years and making a practically working system with reasonable repetition rates an even more distant prospect.

In this paper, we identify for the first time a realistic RPA scheme for current laboratory lasers—based on the use of circular polarization to effectively couple the laser to the entire foil. Simulations using one dimensional (1D) and 2D particle in cell (PIC) simulations predict a step change in the performance of laser based proton and ion accelerators—making low

divergence, monoenergetic giga-electron-volt beams a realistic prospect. Comparisons with the analytical model suggest that we have indeed identified a scheme in which RPA is the dominant interaction.

This paper has four main parts: a discussion of the basic mechanism of our new scheme and comparisons to the scaling predicted by the analytical RPA model, a discussion of the ion energy scaling, some of the practical limits (failure modes) and a discussion of the 2D calculations. The majority of the simulations has been carried out using the electromagnetic (EM) PIC method with one spatial and three momentum dimensions (1D3P). Higher dimensional effects have been addressed by 2D3P calculations using the OSIRIS code [24].

2. Theory

The theoretical starting point for this work is the 1D model of RPA [21, 25]. The 1D relativistic equation of motion for an illuminated foil is derived by first noting that the intensity of the incident radiation in the instantaneous rest (primed) frame of the foil is $I'/I = (1 - v/c)/(1 + v/c)$ where v is the foil velocity. Since the three-force is colinear with the foil velocity, $f'_x = f_x$. One therefore obtains the following equation of motion:

$$\frac{\mathrm{d}p}{\mathrm{d}t} = \frac{2I}{c}\frac{\sqrt{p^2 + \sigma^2 c^2} - p}{\sqrt{p^2 + \sigma^2 c^2} + p}, \tag{1}$$

where p is the areal momentum of the foil and σ is the areal mass of the foil. The most elegant way to integrate equation (1) is to seek a solution of the form,

$$p = \sigma c(\sinh(\psi) - 1/4\sinh(\psi)). \tag{2}$$

One then immediately finds that:

$$\psi = \tfrac{1}{3}\sinh^{-1}\left[\frac{6It}{m_i n_i l c^2} + 2\right], \tag{3}$$

where we have written the foil areal mass as $\sigma = m_i n_i l$ (m_i is the ion mass, n_i the ion density and l is the foil thickness). The momentum of an individual ion is then given by $p_i = m_i c(\sinh(\psi) - 1/4\sinh(\psi))$.

If one illuminates at a constant intensity of $I = 2 \times 10^{21}\,\mathrm{W\,cm^{-2}}$ for 400 fs, and the foil has an areal mass of $5 \times 10^{-5}\,\mathrm{kg\,m^{-2}}$ (a 50 nm thick carbon foil at $1000\,\mathrm{kg\,m^{-3}}$), then one finds that the resultant energy per carbon ion is 5.5 GeV. This is a considerable energy by the standards of most experimental observations, indeed it is well in excess of the 1–2 GeV required for certain medical applications. Note that the model implies that the energy spectrum must be intrinsically monoenergetic, because the model makes the assumption that the force applies to the entire foil and that the foil stays intact.

Substantial caution, however, needs to be applied, since this theory makes the assumption that the laser momentum is efficiently coupled directly to the ion population. Certain conditions will have to be met for this assumption to be valid. The laser primarily interacts with the plasma electrons, and usually the heating of the electrons leads to sheath acceleration dominating. This prevents the entire foil from being uniformly accelerated. For any RPA scheme it is essential that the electric field is dominated by a single positive spike (front and back sheaths must be small

in comparison). This electric field can accelerate all of the ions as single object, which is what equation (1) assumes. This magnitude of this spike must be approximately $E_x = F_{\mathrm{rad}}/en_{\mathrm{e},0}l$ for RPA to dominate (this also implies that the electrons are in force balance), otherwise equation (1) will not model the foil motion. If the size of the spike is comparable to the foil thickness then, from Gauss' law, one finds that the electron and ion densities on each side of the spike must satisfy $2I\epsilon_0/\mathrm{e}^2 n_{\mathrm{e},0}cl^2 \approx |Zn_{\mathrm{i}} - n_{\mathrm{e}}|$. For $I = 10^{21}\,\mathrm{W\,cm^{-2}}$ and $l = 100\,\mathrm{nm}$ one concludes that about half the electrons from one side of the foil need to be moved into the other, and this must be sustained in a quasi-static fashion. This leads one to suspect that circular polarization must be critical, as this will provide a constant ponderomotive expulsion which can sustain this large charge displacement quasi-statically, whereas one suspects that the oscillating ponderomotive force of a linearly polarized pulse will not be able to do this.

3. Simulation results

The challenge is then to find an interaction regime in which these conditions are met, and competing mechanisms (e.g. TNSA) are suppressed. Our results show that this can be achieved by illuminating a solid target with ultra high contrast pulses with circular polarization. In the case of circular polarization the electron dynamics are substantially different. In particular, the ponderomotive pressure no longer oscillates through zero twice per optical cycle. Instead the ponderomotive pressure becomes slowly varying and follows the shape of the intensity envelope. This allows the strong, sustained, expulsion of electrons at lower intensities than with linear polarization which results in weaker expulsion at a given intensity. In a circularly polarized interaction at normal incidence, the periodic expulsion (at frequency 2ω) of relativistic electrons is suppressed and consequently there is no relativistic electron current reaching the target surfaces. The sheath fields responsible for TNSA acceleration are therefore also strongly suppressed allowing RPA to dominate at intensities that are feasible with current laser systems. Achieving RPA using linear polarization relies on exploiting the stronger intensity scaling of RPA versus TNSA and requires the intensity to be increased until RPA dominates the interaction. Unfortunately, this only occurs for laser parameters which are orders of magnitude above the current state of the art [23].

In numerical simulations it is observed that, initially a strong expulsion of electrons occurs in a very thin region. As the spike in the electric field accelerates ions out of this thin region and the critical surface retreats along with the ions the laser begins to penetrate beyond the initial target surface. The ions behind this initial layer are then accelerated similarly. This particular process appears to be very similar to that described by Macchi *et al* [26]. However, as the foil is very thin, eventually the entire ion population is accelerated in this way and has achieved a net positive momentum. Then the ions that originated from the front surface are eventually overtaken and re-accelerated. This repeats in cyclic fashion.

It should be stressed that Macchi *et al* did not consider or demonstrate the possibility of an entire foil being accelerated in the RPA regime. Macchi *et al* concluded that their scheme could produce 'moderate' energy ions, whereas this work demonstrates that this can easily be extended to produce high energy ions. We should also address the matter of the statement in the later work of Esirkepov *et al* [27] that a 'transition' into the RPA regime begins around $5 \times 10^{21}\,\mathrm{W\,cm^{-2}}$. Exactly how a smooth transition occurs was not made clear. In the RPA mechanism there is no dependence on the ion charge or laser wavelength, for example, whereas there is a strong dependence the TNSA mechanism. Nor was it demonstrated that strongly

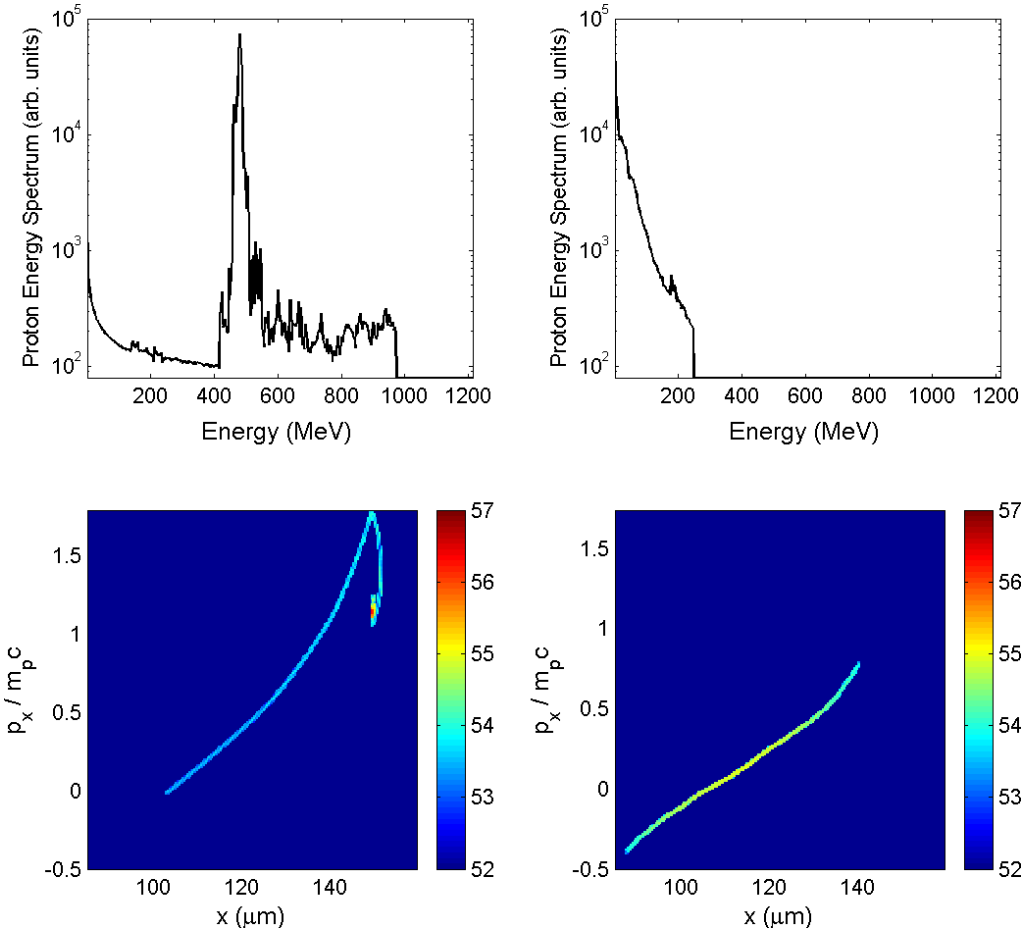

Figure 1. Top left panel: proton energy spectrum after 400 fs in the standard run. Bottom left panel: $\log_{10} p_x - x$ proton phase space at 400 fs in standard run. Top right panel: proton energy spectrum for identical parameters but with linear polarization. Bottom right panel: $\log_{10} p_x - x$ proton phase space at 400 fs in linear polarization run. In the case of circular polarization the foil is accelerated as a whole, leading to a narrow energy spectrum, whereas in the case of linear polarization the foil violently decompresses and produces a broad energy spectrum.

monoenergetic spectra could be obtained early in this transition. In contrast to that work, what we are demonstrating here is that a *complete* switch from the TNSA to the RPA regime can be obtained at intensities around $10^{21}\,\mathrm{W\,cm^{-2}}$. This is illustrated clearly by figure 1. The work of Zhang *et al* [28] may well describe a similar mechanism, although in this paper we describe a regime in which much higher energy ions are produced, and we demonstrate that an RPA model correctly describes the scaling.

The specifics of the 1D EM PIC simulations are now reported. This considered a 150 nm foil consisting of protons at density of $8 \times 10^{28}\,\mathrm{m^{-3}}$ with a corresponding electron density to give initial charge neutrality with an initial electron and ion temperature of 10 keV (to ensure a reasonable time-step). The front surface is initially located at 105 μm on the grid. A circularly

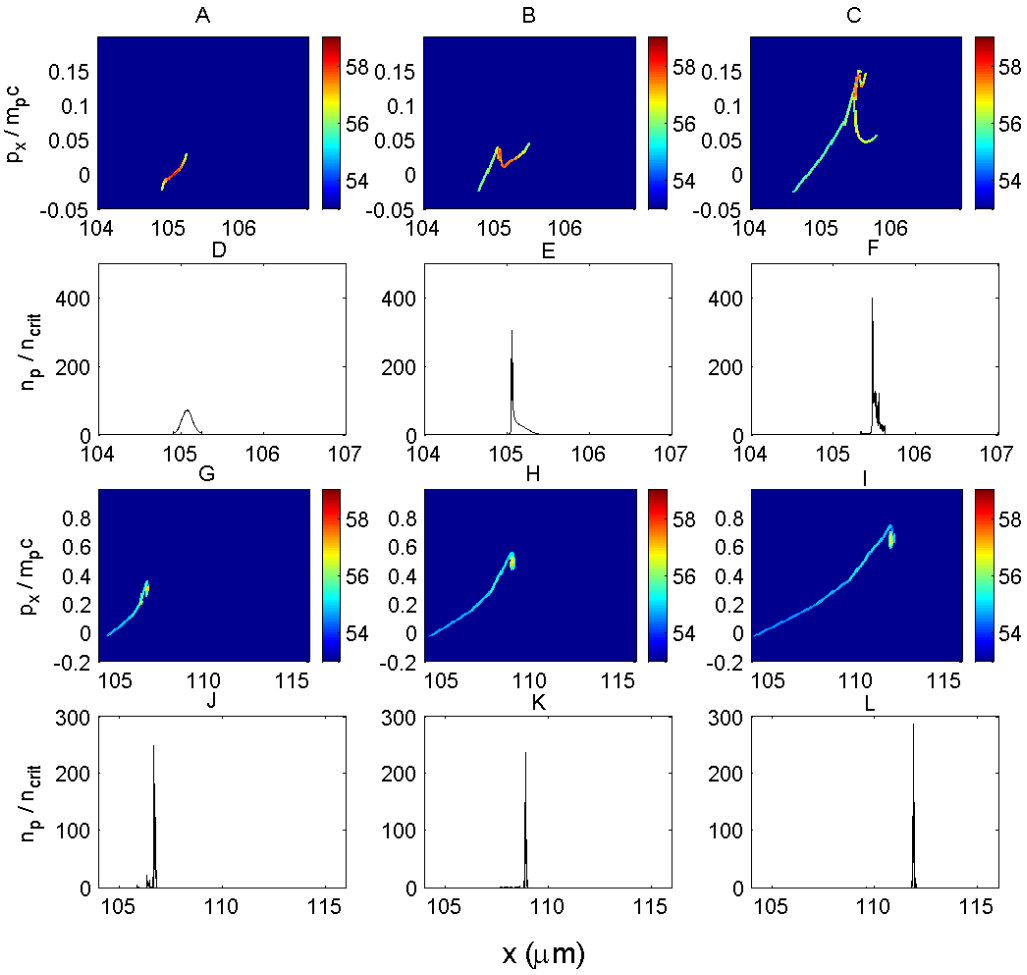

Figure 2. (A–C and G–I) Proton $\log_{10} p_x - x$ phase space plots in the standard run. (D–F and J–L) Proton density ($n_\mathrm{p}/n_\mathrm{crit}$) profiles in the standard run. Times are: A and D = 20 fs, B and E = 40 fs, C and F = 60 fs, G and J = 80 fs, H and K = 100 fs and I and L = 120 fs. Note the changes in scale. It can be seen that, after 60 fs, the foil moves as a whole with only a very small amount of material being left as trailing mass.

polarized EM wave with $\sin^4(t)$ with a full width half maximum (FWHM) pulse duration of 64 fs and the peak intensity is $2 \times 10^{21}\,\mathrm{W\,cm^{-2}}$ is incident on the foil. This constitutes our standard calculation, which we carry out up to 400 fs. As anticipated the foil is accelerated as a whole and the spectrum shows that almost the entire ion population is concentrated in a monoenergetic spectral peak at 485 MeV (figure 1 (top left panel)).

The aforementioned evolution of the proton phase space is illustrated by figure 2. The corresponding proton density profiles are also shown. This shows how the ions are initially accelerated at the front surface and are driven through the target. The electric field consists of a single positive spike, which is created by a very strong charge displacement at the front of the ion mass. It is during the time, from 20–60 fs, that the phase space evolution has many similarities to the process described by Macchi *et al*. It is from 60 fs onwards that the cyclic

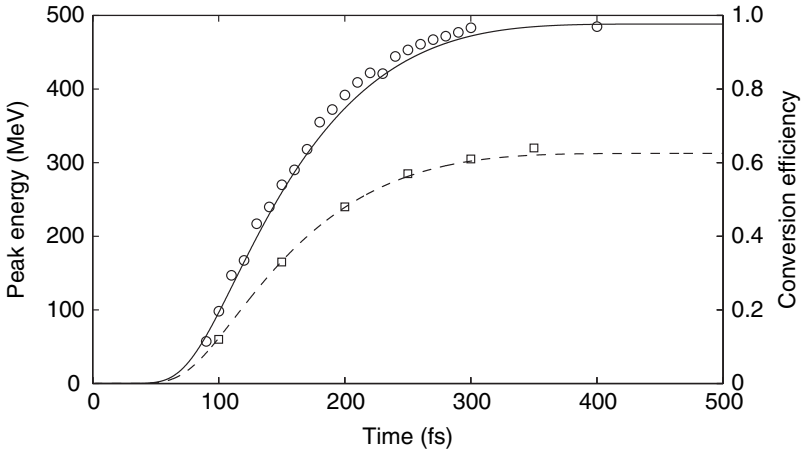

Figure 3. Comparison of semi-analytic model (solid line) with peak proton energy in the standard run (circles). Conversion efficiency also shown for both the model (dashed line) and standard run (squares).

acceleration of the foil mass occurs, i.e. after the ions from the front surface have been pushed through the rear surface. At these later times the phase space shows a distinct 'head', where the majority of the ion mass is concentrated, and a 'tail' which contains a very low amount of trailing mass.

The results of the simulation are in excellent agreement with a semi-analytical RPA model as can be seen in figure 3, where the prediction of a semi-analytical model for the energy of the spectral peak (i.e. modal energy) and the conversion efficiency (reaching $>60\%$) is compared to the simulation results. The semi-analytic model is based on integrating equation (1) and an equation which specifies the intensity profile (i.e. $I = I(t)$). The position of the foil, $x_{\text{foil}}(t)$, must also be tracked so one has two first-order differential equations and a pulse specification equation which can be integrated numerically very quickly. The peak energy in the simulation is always slightly higher than that predicted by the semi-analytic model. This is because the foil loses some mass in the form of 'trailing mass' that gets left behind as the foil is accelerated.

It is also interesting to assess factors that do not play any role in the analytic model. Firstly, there is the matter of wavelength. This is absent from the analytic model (as seen in equation (1), and this contrasts greatly with TNSA in which ion energy scaling depends on $(I\lambda^2)^{1/2}$ [18]. On repeating the standard run with $0.5\,\mu$m light, it is found that the results differ less than 10%, however, this must become important in the limit where the wavelength becomes so short that the foil is transparent. Secondly, there is the matter of the ion charge, or the charge to mass ratio of the ions, which is also absent from the analytic model, but is not in TNSA [6]. When the standard run is repeated for particles with $A = 1$ and $Z = 2$ the results also differ by less than 10%. Thus it has been shown that the radiation pressure model is an excellent explanation of these simulation results both in terms of the peak proton energy evolution with time and the fact that this mechanism has only a very weak dependence on wavelength or ion charge.

It is instructive to contrast these results with the results obtained using linear polarization in otherwise identical conditions. The constant expulsion of electrons is not achieved and this acceleration mechanism fails giving way to TNSA (figure 1 (top right panel)), in agreement with experimental evidence [29]. The phase space plots in figure 1 (bottom left and right panels) also

show that the acceleration is completely different in the two cases. We should re-iterate that this shows that the change in laser polarization results in a complete switch between two completely different acceleration regimes. Furthermore it should be noted that when simulations are carried out under different conditions (such as for different foil thicknesses and intensities as reported in section 4) the same applies—repeating the simulation with linear polarization results in the mechanism reverting to TNSA and a broad energy distribution. This is in agreement with the conclusions drawn at the end of section 2.

4. Discussion

The semi-analytical model allows the dependence on the final peak proton energy on foil thickness d and intensity to be estimated very accurately. These scale as $\propto d^{-1}$ and $\propto I$ (for non-relativistic foil velocities), respectively. This was shown to be the case by carrying out a set of 1D PIC runs over a wide range of parameters, the results of which are shown in (figure 4). As in the case of the standard run, the agreement with the semi-analytic model is excellent. Monoenergetic spectra are still obtained in each case, although the relative energy spread is larger the lower the final proton energy. The highest proton energies are thus achieved for thin foils at high irradiance with 1 GeV protons predicted for intensities $3 \times 10^{21}\,\mathrm{W\,cm^{-2}}$ and $d = 150$ nm. These simulations also show that the scheme has the potential to accelerate a large *total* number of ions, $N = n_\mathrm{i} l A$, where A is the actual area of the foil that will be accelerated due to the finite size of the laser spot. Even if the area accelerated has a radius of 1–2 μm one expects to accelerate 10^{10} ions, and if this radius is increased to 4–5 μm then one expects to accelerate $>10^{11}$ ions.

To assess how robust this scheme was, several potential real-life failure modes were investigated. Clearly, the foil must be thick enough and have a sufficiently high density to avoid becoming transparent. In the case of the standard run (1 μm wavelength) this begins to occur below 100 nm (see figure 4 (left panel)), suggesting that the acceleration of ultrathin foils at very high intensities is only possible using longer wavelengths. Complete failure for the standard run parameters was found to occur at 20 nm foil thickness. The effects of the pulse being elliptically, as opposed to perfectly circularly, polarized were also investigated. It was found that a deviation from circular to ellipticities of 1.5 : 1 to 2 : 1 had little significant effect.

A critical failure mode that is relevant to any RPA scheme is also highlighted for targets consisting of multiple ion-species. Since the electric field will be determined by the electron density $n_\mathrm{e} = Z_1 n_{\mathrm{i},1} + Z_2 n_{\mathrm{i},2}$, and the equation of motion for each ion species will be given by:

$$\frac{\mathrm{d}p_{\mathrm{i},k}}{\mathrm{d}t} = \frac{Z_k n_{\mathrm{i},k}(2I/c)[(1 - v/c)/(1 + v/c)]}{(Z_1 n_{\mathrm{i},1} + Z_2 n_{\mathrm{i},2})}. \tag{4}$$

This scenario was examined by comparing simulations identical to the standard run, except that the protons were replaced by a mixture of protons and C^{6+} each at a density of $4 \times 10^{28}\,\mathrm{m^{-3}}$. The acceleration of the C^{6+} ions was not significantly affected and reached a final energy of 280 MeV compared to 339 MeV predicted by the semi-analytic model. By contrast the protons were badly affected and only reached energies of 20–40 MeV compared to 485 MeV achieved in the standard run. Although the species separated, the foil was not destroyed in this instance. However, the protons can only ever be accelerated to the extent that they are co-moving with the heavy ions, hence achieve a greatly reduced energy. Therefore, accelerating protons using

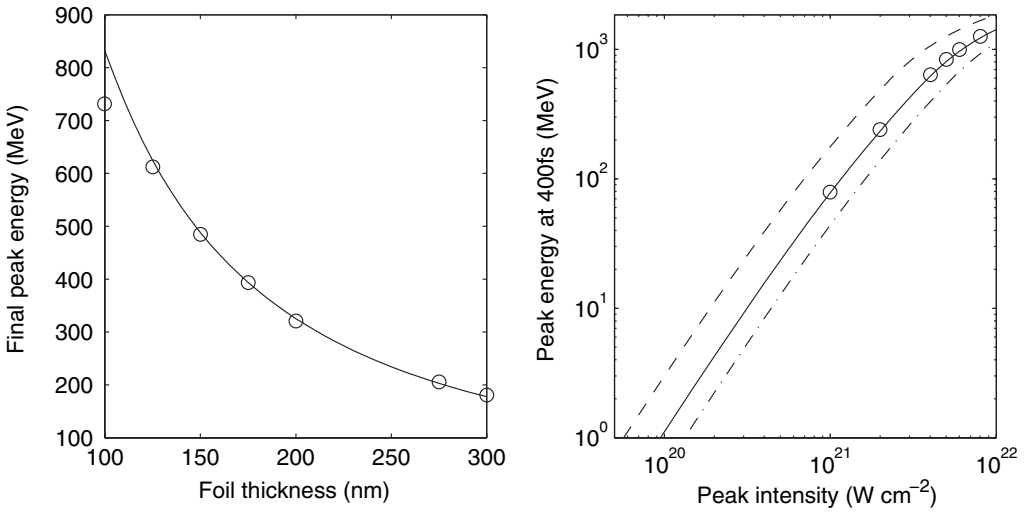

Figure 4. Peak proton energy against foil thickness (left panel) and peak intensity (right panel) in both PIC simulations (circles) and semi-analytic model (lines). Dashed: 150 nm, solid: 250 nm and dash-dot: 350 nm foil thickness in right panel.

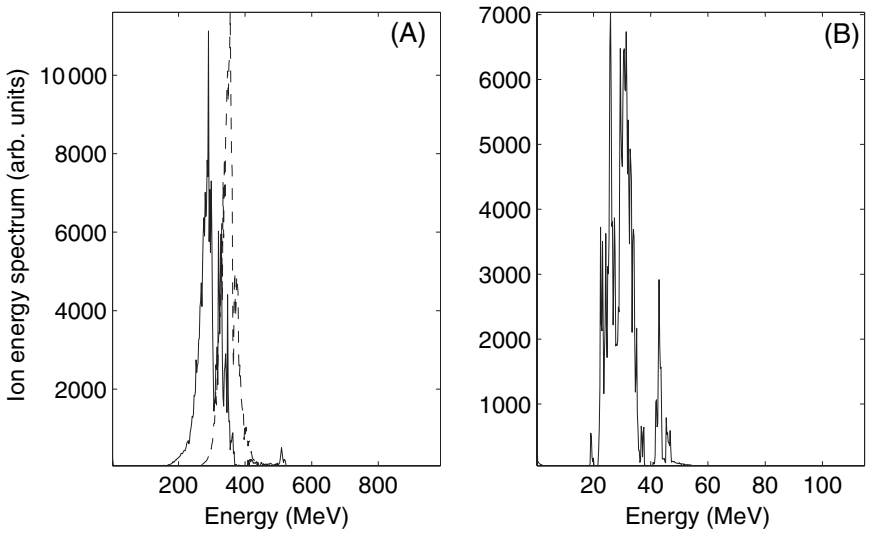

Figure 5. Left panel: C^{6+} energy spectra in 1 : 1 C^{6+} : H^{+} simulations (solid) and pure C^{6+} simulation (dashed). Right panel: proton energy spectrum in 1 : 1 C^{6+} : H^{+} simulation.

this scheme presents technical challenges, but the acceleration of heavy ions is easier as proton contamination is uncritical, which stands in stark contrast to the TNSA mechanism.

This scenario was examined by comparing simulations identical to the standard run, the results of which are shown in figure 5. The run is identical to the standard run, except that the protons have been replaced by a mixture of protons and C^{6+} each at a density of $4 \times 10^{28}\,\mathrm{m}^{-3}$. The results for a simulation where the protons are not present is also shown. The energy spectra

are taken from the simulation at 400 fs in all three cases. The energy spectrum of the C^{6+} ions in figure 5 show that the C^{6+} ions are not badly affected by this failure mode. Note that the semi-analytic model predicts an energy of 339 MeV for the C^{6+} only case. The protons are undesirable, however, as a lower peak energy is achieved. The protons are badly affected by this failure mode, however, as shown by the proton energy spectrum in figure 5 in which proton energies between 20 and 40 MeV are achieved which should be compared to the 485 MeV achieved in the standard run. In the simulation it is observed that the protons move ahead and separate from the C^{6+} ions. The accelerating electric field is much lower in the proton-only region. The C^{6+} ions subsequently overtake the protons, and the protons are accelerated again. The result is that the protons are only ever accelerated to such an extent that they can move at approximately the same speed as the carbon ions, and thus only low proton energies are achieved. Therefore, accelerating protons using this scheme presents technical challenges, but the acceleration of heavy ions is easier since proton contamination is unimportant. This stands in stark contrast to the TNSA mechanism in which the presence of a light ion population strongly inhibits the acceleration of heavy ions.

Since the foils must be very thin for efficient RPA to take place, pulse contrast becomes a critical issue. Recent experiments [30] have demonstrated that ultrathin foils as thin as 50 nm can remain intact until the peak of a 50 fs, 10^{19} W cm^{-2} pulse arrives. This demonstrates that sufficiently high contrast can be achieved, although plasma mirrors might be required at the highest intensities [31]. However, there will inevitably be some decompression as a result of the rising edge of even ultra-high contrast pulses for such thin foils. To test that the scheme is not dependent on the precise density profile, simulations were performed on foils that were decompressed by a factor of two in density to simulate the effect of the rising edge of the pulse. This also showed very little effect on the overall acceleration of the foil.

5. 2D simulations

Finally, to assess the impact of higher dimensional effects, 2D3P OSIRIS simulations were performed. These simulations used a grid of 4000 cells along the laser axis and 8000 cells transversely (16 μm $\times$ 32 μm). The foil was 100 nm thick consisting of electrons and protons (400 particles per cell at a density of $100n_{\mathrm{crit}}$, initial electron temperature of 3 keV). The normally incident laser pulse was circularly polarized with a peak a_0 of 34 and was approximately Gaussian with 31 fs FWHM duration. The transverse spatial distribution is a fourth-order supergaussian ($I \propto \exp(-(r/r_0)^4)$) with a $1/e$ width of 13 μm—corresponding to focusing a top-hat laser beam outside the Rayleigh range. This shape allows quasi 1D dynamics to be maintained in the 2D simulation, by ensuring that the length over which the acceleration takes place is smaller than the transverse dimension over which the laser intensity varies negligibly. This shape contributes greatly to the flat acceleration profile; a normal Gaussian gives a very curved shape to the foil and produces a broad energy spectrum with reduced peak energy.

Figure 6 shows both a plot of the ion density at 64 fs, and the energy spectrum at different times. The divergence angle of the protons (within $y = 10$–20 μm) is less than 4°. In 1D, taking the on-axis intensity, the semi-analytic model predicts peak energy of 260 MeV, compared to a peak energy of 240 MeV in the 2D calculation. This shows that 2D effects do not substantially affect the acceleration process. As one would expect, the foil shows some transverse Rayleigh Taylor like instability which begins to result in spectral broadening at late times. It should be

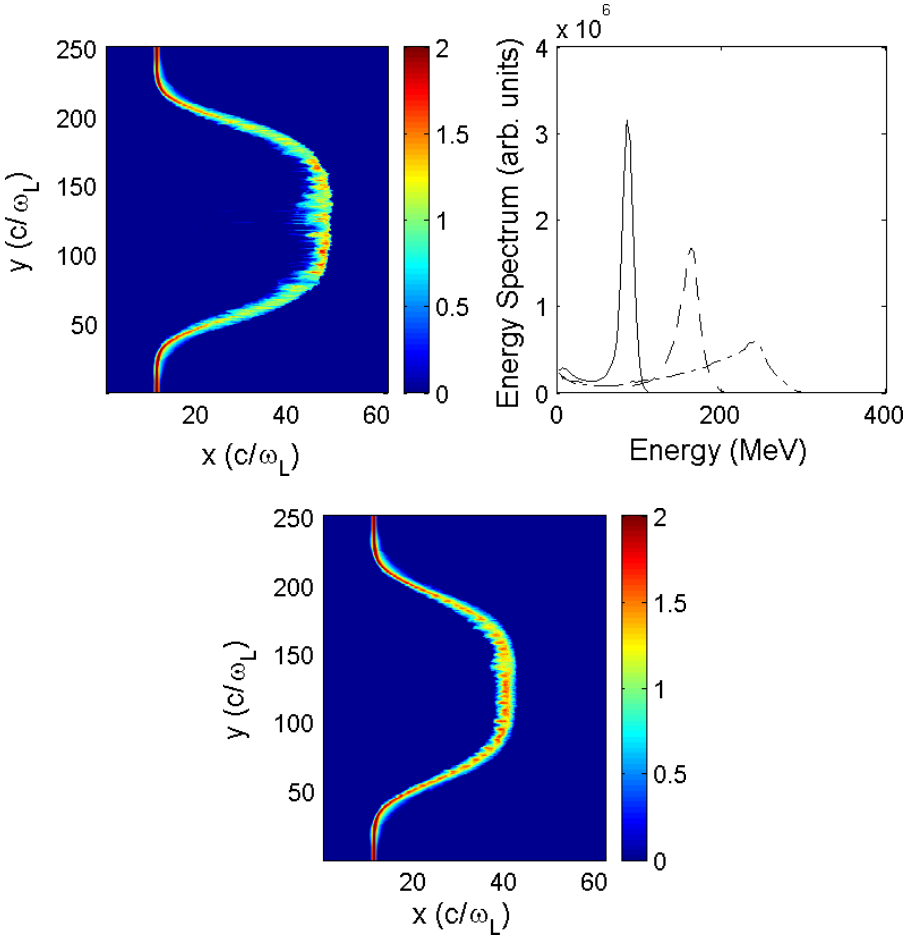

Figure 6. Results from 2D OSIRIS simulation: Top left panel: proton density ($\log_{10}(n_p/n_{crit})$) at 64 fs. Bottom panel: proton density ($\log_{10}(n_p/n_{crit})$) at 64 fs in simulation with zero initial electron temperature. Top right panel: proton energy spectra at 53 (solid), 64 (dashed) and 75 (dash-dot) fs.

emphasized that the growth rate and hence the scale of spectral broadening is overestimated by the current simulations. It was found that these effects decrease substantially as the number of particles per cell is increased and initial temperature is decreased. The effect of setting the initial electron temperature to zero is also shown in figure 6. A further increase in the number of particles per cell and a reduction of cell size (allowing a lower initial temperature) is expected to reduce these effects further. However, these simulations represent the limit of our computational capacity.

6. Summary

In summary, it has been demonstrated that laser based ion acceleration based on radiation pressure is viable at intensities around 10^{20}–10^{21} W cm^{-2} using high contrast, circularly polarized pulses. This produces highly energetic, monoenergetic ions very efficiently. The mechanism has been identified as a RPA on the basis of a semi-analytic model. The

semi-analytic model agrees extremely well with the simulation results and thus accurately predicts the energy scaling. RPA of ions at intensities achievable with the latest laser technology represents a step change in the quality and performance of laser-ion acceleration.

Acknowledgments

We are grateful for the use of computing resources provided by STFC's e-Science facility. M Zepf is supported by the Royal Society.

References

[1] Clark E L *et al* 2000 Energetic heavy-ion and proton generation from ultraintense laser-plasma interactions with solids *Phys. Rev. Lett.* **85** 1654
[2] Maksimchuk A *et al* 2000 Forward ion acceleration in thin films driven by a high-intensity laser *Phys. Rev. Lett.* **84** 4108
[3] Snavely R A *et al* 2000 Intense high energy proton beams from petawatt-laser irradiation of solids *Phys. Rev. Lett.* **85** 2945
[4] Hatchett S *et al* 2000 *Phys. Plasmas* **5** 2076
[5] Esirkepov T Z *et al* 2002 Proposed double-layer target for the generation of high-quality laser-accelerated ion beams *Phys. Rev. Lett.* **89** 175003
[6] Mora P 2003 Plasma expansion into vacuum *Phys. Rev. Lett.* **90** 185002
[7] Schwoerer H *et al* 2006 Laser-plasma acceleration of quasi-monoenergetic proton from microstructured targets *Nature* **439** 445
[8] Hegelich M *et al* 2006 Laser acceleration of quasi-monoenergetic MeV ion beams *Nature* **439** 441
[9] Toncian T *et al* 2006 *Science* **312** 410
[10] Cowan T *et al* 2004 Ultralow emittance, multi-MeV proton beams from a laser virtual-cathode plasma accelerator *Phys. Rev. Lett.* **92** 204801
[11] Borghesi M *et al* 2004 Multi-MeV proton source investigations in ultra-intense laser-foil interactions *Phys. Rev. Lett.* **92** 055003
[12] Mackinnon A J *et al* 2002 Enhancement of proton acceleration by hot electron recirculation in thin foils irradiated by ultraintense laser pulses *Phys. Rev. Lett.* **88** 215006
[13] Tabak M *et al* 1994 Ignition and high gain with ultrapowerful lasers *Phys. Plasmas* **1** 1626
[14] Roth M *et al* 2001 *Phys. Rev. Lett.* **86** 436
[15] Temporal M *et al* 2002 Numerical study of fast ignition of ablatively imploded deuterium-tritium fusion capsules by ultra-intense proton beams *Phys. Plasmas* **9** 3098
[16] Borghesi M *et al* 2005 Plasma ion evolution in the wake of a high-intensity ultrashort laser pulse *Phys. Rev. Lett.* **94** 195003
[17] Bychenkov V Yu 2004 Ion acceleration in expanding multispecies plasmas *Phys. Plasmas* **11** 3242
[18] Wilks S C *et al* 2001 Energetic proton generation in ultraintense laser-solid interactions *Phys. Plasmas* **8** 542
[19] Sentoku Y *et al* 2003 High energy proton acceleration in interaction of a short laser pulse with dense plasma target *Phys. Plasmas* **10** 2009
[20] Kemp A J and Ruhl H 2005 Multispecies ion acceleration off laser-irradiated water droplets *Phys. Plasmas* **12** 033105
[21] Marx G. 1966 Interstellar vehicle propelled by terrestrial laser beam *Nature* **211** 22
[22] Lindl J *et al* 2004 The physics basis for ignition using indirect-drive targets on the national ignition facility *Phys. Plasmas* **11** 339
[23] Esirkepov T *et al* 2004 Highly efficient relativistic-ion generation in the laser-piston regime *Phys. Rev. Lett.* **92** 175003

[24] Lee S 1988 *Phys. Rev.* E **61** 7014
[25] Simmons J F L and McInnes C R 1993 *Am. J. Phys.* **61** 205
[26] Macchi A *et al* 2005 Laser acceleration of ion bunches at the front surface of overdense plasmas *Phys. Rev. Lett.* **94** 165003
[27] Esirkepov T *et al* 2006 *Phys. Rev. Lett.* **96** 105001
[28] Zhang X *et al* 2007 *Phys. Plasmas* **14** 073101
[29] McKenna P *et al* 2006 *Phil. Trans. R. Soc.* A **364** 711
[30] Neely D *et al* 2006 *Appl. Phys. Lett.* **89** 021502
[31] Dromey B *et al* 2004 *Rev. Sci. Instrum.* **75** 645